

The Structure of Formaldehyde-Inhibited Xanthine Oxidase Determined by 35 GHz ^2H ENDOR Spectroscopy

Muralidharan Shanmugam,[†] Bo Zhang,[‡] Rebecca L. McNaughton,[†] R. Adam Kinney,[†] Russ Hille,^{*,‡} and Brian M. Hoffman^{*,†}

Chemistry Department, Northwestern University, Evanston, Illinois 60208-3113, and Department of Biochemistry, University of California, Riverside, California 95521

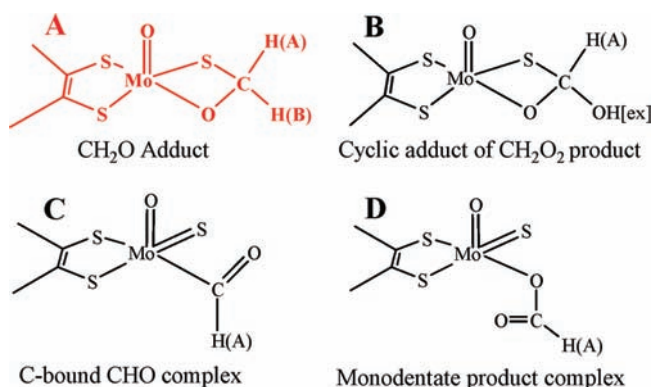
Received July 20, 2010; E-mail: bmh@northwestern.edu

Abstract: The formaldehyde-inhibited Mo(V) state of xanthine oxidase (**I**) has been studied for four decades, yet it has not proven possible to distinguish unequivocally among the several structures proposed for this form. The uniquely large isotropic hyperfine coupling for ^{13}C from CH_2O led to the intriguing suggestion of a direct Mo–C bond for the active site of **I**. This suggestion was supported by the recent crystal structures of glycol- and glycerol-inhibited forms of aldehyde oxidoreductase, a member of the xanthine oxidase family. ^1H and ^2H ENDOR spectra of **I**($\text{C}^{1,2}\text{H}_2\text{O}$) in $\text{H}_2\text{O}/\text{D}_2\text{O}$ buffer now have unambiguously revealed that the active-site structure of **I** contains a CH_2O adduct of Mo(V) in the form of a four-membered ring with S and O linking the C to Mo and have ruled out a direct Mo–C bond. Density functional theory computations are consistent with this conclusion. We interpret the large ^{13}C coupling as resulting from a “transannular hyperfine interaction”.

Xanthine oxidase is a molybdoenzyme that catalyzes the oxidative hydroxylation of a variety of heterocyclic and aldehyde substrates, including the physiological substrates hypoxanthine and xanthine.¹ Of the large number of EPR-active Mo(V) intermediates exhibited by this enzyme,² one of the most intriguing is the CH_2O -inhibited Mo(V) form (**I**) first described by Bray and co-workers.³ Its most remarkable feature, which was revealed by Howes and co-workers,^{4,5} is the presence of a carbon derived from CH_2O that EPR and ENDOR spectroscopies show to have a uniquely large ^{13}C isotropic hyperfine coupling, $a_{\text{iso}}(^{13}\text{C}) \approx 43.0$ MHz. This value contrasts with the 5-fold smaller coupling for the Mo–O– ^{13}C of the “2-hydroxy-6-methyl-purine (HMP) very rapid” form ($a_{\text{iso}} = 7.9$ MHz).⁶ Although **I** has been studied for 40 years, it has not proven possible to distinguish unequivocally among the viable candidates for its structure (Scheme 1).^{5,7–13}

The large isotropic ^{13}C hyperfine coupling for **I** led Howes and co-workers to the intriguing suggestion that it contains a CHO fragment with a direct Mo–C bond (**C** in Scheme 1).^{4,5} This suggestion recently received support from the crystal structures of glycol- and glycerol-inhibited forms of aldehyde oxidoreductase (AOR), a member of the xanthine oxidase family.⁷ These structures exhibit Mo–C bond distances of 2.36 and 2.72 Å, respectively, the former in particular being suggestive of direct Mo–C bonding interactions. In contrast, analysis of the smaller ^{13}C coupling for a substrate-derived species bound to Mo(V) of the “very rapid” state of xanthine oxidase indicated that there was no direct Mo–C bond,⁶ and this was confirmed by recent crystal structures for that intermediate.^{14,15}

Scheme 1



We here report that ^1H and ^2H ENDOR spectra of **I**($\text{C}^{1,2}\text{H}_2\text{O}$) prepared¹⁶ in $\text{H}_2\text{O}/\text{D}_2\text{O}$ buffer rule out all of the models proposed for the active-site structure of **I** (Scheme 1) except for model **A**, a four-membered cyclic adduct of CH_2O with S and O linking the C to Mo. Density functional theory (DFT) calculations are consistent with the ENDOR finding that **A** rather than the direct Mo–C bond of **C** represents the structure for the active site of **I**.

The reported X-band EPR spectrum of **I**($^{13}\text{C}^1\text{H}_2\text{O}$) in H_2O shows a doublet splitting from the ^{13}C nucleus, with each line further split into a doublet from a single proton derived from CH_2O .⁴ The 35 GHz echo-detected EPR spectrum of **I**($^{12,13}\text{C}^1\text{H}_2\text{O}$) in H_2O shows the ^{13}C doublet from $^{13}\text{C}^1\text{H}_2\text{O}$, but the ^1H splitting is not observed (Figure S1).^{17,18} The EPR spectrum of **I**($^{12,13}\text{C}^1\text{H}_2\text{O}$) further shows hyperfine splitting from $^{95,97}\text{Mo}$ (natural abundances: ^{95}Mo , 15.9%; ^{97}Mo , 9.6%). The g_1 and g_3 splittings are observable in both the X- and Q-band spectra; those associated with g_2 are resolved only in the Q band spectrum (Figure S1). Simulations of the EPR spectra gave principal values of the **g** tensor and values of the components of **A** for the ^{13}C of CH_2O that agree with those of Howes and co-workers: **g** = [1.988, 1.974, 1.948], **A**(^{13}C) = [51.5, 40, 40] MHz, $a_{\text{iso}} = 43.8$ MHz.

Figure 1 presents 35 GHz Davies ^1H and $^{95,97}\text{Mo}$ (top) and Mims ^2H (bottom) ENDOR spectra collected for **I**($^{12}\text{C}^{1,2}\text{H}_2\text{O}$) in $\text{H}_2\text{O}/\text{D}_2\text{O}$ near g_2 , the magnetic field corresponding to the maximum EPR intensity. The ^1H Davies spectra of **I**($\text{C}^1\text{H}_2\text{O}$) in H_2O and D_2O are essentially the same (traces **A**), both exhibiting an ^1H doublet centered at the ^1H nuclear Larmor frequency and split by $A \approx 13$ MHz. This doublet is absent in the spectrum of **I**($\text{C}^2\text{H}_2\text{O}$) in H_2O (trace **B**) and thus is associated with a proton, $^1\text{H}_A$, derived from CH_2O . The ^1H doublet in Figure 1 rides on $^{95,97}\text{Mo}$ ENDOR signals and is more clearly seen in the difference spectrum **A**–**B** obtained by subtraction of the spectrum of **I**($\text{C}^2\text{H}_2\text{O}$) (**B**) from that of **I**($\text{C}^1\text{H}_2\text{O}$) (**A**).

[†] Northwestern University.

[‡] University of California, Riverside.

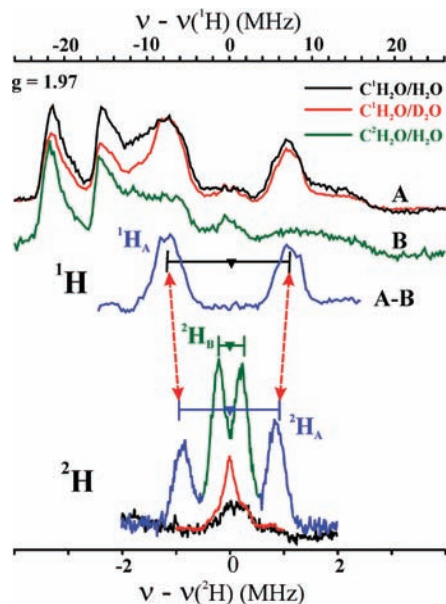


Figure 1. (top) Davies ^1H and $^{95.97}\text{Mo}$ (A, B) ENDOR spectra (35 GHz) of $\text{I}(\text{C}^2\text{H}_2\text{O})$ in H_2O and D_2O buffers. (bottom) Mims ^2H ENDOR spectra (35 GHz) of $\text{I}(\text{C}^2\text{H}_2\text{O})$ in H_2O (green/blue), $\text{I}(\text{C}^1\text{H}_2\text{O})$ in H_2O (black) and D_2O (red) buffer. Horizontal bars indicate hyperfine splittings for $^1\text{H}_{\text{A,B}}$ nonexchangeable protons. Conditions: $g = 1.97$; $T = 2$ K. Davies: π -pulse = 80 ns, $\tau = 600$ ns, repetition time = 50 ms, 34.84 GHz. Mims ^2H : $\pi/2$ pulse = 50 ns, $\tau = 800$ ns, repetition time = 50 ms, 34.87 GHz.

The $^1\text{H}_{\text{A}}$ doublet is lost and is replaced by a corresponding $^2\text{H}_{\text{A}}$ signal when $\text{C}^2\text{H}_2\text{O}$ is the substrate. ^2H ENDOR spectra of $\text{I}(\text{C}^2\text{H}_2\text{O})$ in H_2O by both Davies (not shown) and Mims (Figure 1, lower) techniques exhibit a $^2\text{H}_{\text{A}}$ doublet without resolved quadrupole splitting. The hyperfine interaction, $\text{A}(^2\text{H}_{\text{A}})$, corresponds to a smaller value of $\text{A}(^1\text{H}_{\text{A}})$ than that seen directly in the ^1H ENDOR spectrum of $\text{I}(\text{C}^1\text{H}_2\text{O})$ in $\text{H}_2\text{O}/\text{D}_2\text{O}$ because of a substantial isotope effect on the hyperfine couplings.^{19,20} Most importantly, the ^2H Mims spectrum of $\text{I}(\text{C}^2\text{H}_2\text{O})$ in H_2O shows doublets from *both* deuterons derived from the $\text{C}^2\text{H}_2\text{O}$ (Figure 1), a second doublet, denoted $^2\text{H}_{\text{B}}$, plus that from $^2\text{H}_{\text{A}}$.

To test for protons exchangeable with solvent, Mims ^2H ENDOR spectra were collected for $\text{I}(\text{C}^1\text{H}_2\text{O})$ in D_2O and $\text{I}(\text{C}^2\text{H}_2\text{O})$ in H_2O at g_2 (Figure 1, bottom). The nearly featureless ^2H spectrum of $\text{I}(\text{C}^1\text{H}_2\text{O})$ in D_2O shows clearly that there are no exchangeable protons in the active site of **I**.

To confirm that the Mims ^2H spectrum is not significantly distorted by suppression “holes” associated with this technique²¹ and to determine the ^2H hyperfine and quadrupolar tensors, we collected a complete 2D field–frequency ^2H ENDOR pattern of spectra acquired at numerous magnetic fields across the EPR envelope and simulated this pattern with inclusion of the suppression effects (Figure S2 in the Supporting Information).²² At magnetic fields near g_1 , the spectra show the $^2\text{H}_{\text{A}}$ and $^2\text{H}_{\text{B}}$ doublets centered at the ^2H Larmor frequency and split by $A \approx 1.8$ and 0.4 MHz, respectively. The ^2H ENDOR pattern does not change significantly as the field is moved toward g_2 and g_3 , except in intensity, indicating that the hyperfine couplings of $^2\text{H}_{\text{A}}$ and $^2\text{H}_{\text{B}}$ are largely isotropic. The 2D pattern is well-simulated by the 1:1 summation of simulations of $^2\text{H}_{\text{A}}$ and $^2\text{H}_{\text{B}}$, with $\text{A}(^2\text{H}_{\text{A}}) = [1.8, 1.8, 1.9]$ MHz and $\text{A}(^2\text{H}_{\text{B}}) = [0.44, 0.4, 0.39]$ MHz. Neither ^2H exhibits quadrupolar splitting ($I = 1$) because of the large ENDOR line widths. As noted above for the g_2 spectrum, the tensor obtained from simulations of the $^2\text{H}_{\text{A}}$ ENDOR pattern only approximately matches that obtained by fitting a 2D ^1H Davies ENDOR pattern for $^1\text{H}_{\text{A}}$ because of an isotope effect on the hyperfine couplings.^{19,20}

The finding that both aldehydic protons of CH_2O are retained in **I** and are nonexchangeably hyperfine-coupled to the $\text{Mo}(\text{V})$ of **I** rules out all of the candidates for the active-site structure of **I** shown in Scheme 1 except the cyclic CH_2O adduct, **A**.

DFT calculations (SI) are consistent with experiment, yielding hyperfine tensors for ^{13}C , $^2\text{H}_{\text{A}}$, and $^2\text{H}_{\text{B}}$ of CH_2O in **A** that all are in satisfactory agreement with the experimentally observed values: $a_{\text{iso}}(^{13}\text{C}) \approx 47.9$ MHz, $\text{A}(^{13}\text{C}) = [53.6, 45.4, 44.6]$ MHz; $\text{A}(^2\text{H}_{\text{A}}) = [4.0, 3.3, 3.0]$ MHz; $\text{A}(^2\text{H}_{\text{B}}) = [0.38, -0.67, -0.72]$ MHz. Most importantly, the carbon-bound CHO complex, model **C**, which is already ruled out by the absence of H_{B} , is calculated to have almost 3-fold and 5-fold smaller ^{13}C and $^1\text{H}_{\text{A}}$ hyperfine couplings, respectively: $a_{\text{iso}}(^{13}\text{C}) \approx 16.1$ MHz, $\text{A}(^{13}\text{C}) = [23.2, 13.4, 11.7]$ MHz; $\text{A}(^2\text{H}_{\text{A}}) = [0.51, -0.43, -0.66]$ MHz.

Why is the ^{13}C coupling so much larger for the carbon bound in the four-membered ring of structure **A**, and not directly coordinated to $\text{Mo}(\text{V})$, than it would be for a carbon directly bonded to the metal ion in **C**? We interpret the large coupling in **A** as resulting from a “transannular hyperfine interaction”.^{23,24} The carbon is in line with a lobe of the half-occupied $\text{Mo}(\text{d}_{xy})$ orbital, and this allows overlap between $\text{Mo}(\text{d}_{xy})$ and orbitals of carbon; the large a_{iso} for ^{13}C corresponds to only $\sim 1.2\%$ spin density in a carbon 2s orbital. This phenomenon was first observed for a phosphorus atom that formed part of four-membered cyclic structures of $\text{Mo}(\text{V})$ and $\text{V}(\text{IV})$ with dialkyl/aryldithiophosphinato ligands.^{23,24} A weaker hyperfine coupling was observed when the ^{31}P is bound to the metal ion directly through a monodentate $\text{M}-\text{O}-\text{P}$ linkage,²⁵ and the same is true for the $\text{Mo}-\text{O}-^{13}\text{C}$ of the “very rapid” intermediate.⁶ Transannular effects may have relevance to a recent proposal of a direct $\text{Fe}-\text{C}$ bond based on a large ^{13}C coupling.²⁶

Finally, regarding the use of distances in the X-ray structure to infer a direct $\text{Mo}-\text{C}$ bond, we note that the DFT-optimized cyclic structure **A** has a $\text{Mo}-\text{C}$ distance of 2.76 Å, which is the same as that found by X-ray diffraction for the glycerol-inhibited form of **AOR**.⁷

Acknowledgment. Support by the NIH (GM 075036, R.H.) and NSF (MCB0723330, B.M.H.) is acknowledged.

Supporting Information Available: One EPR figure, one ENDOR figure, and DFT calculation methods. This material is available free of charge via the Internet at <http://pubs.acs.org>.

References

- Hille, R. *Chem. Rev.* **1996**, *96*, 2757–2816.
- Hille, R. In *Metals in Biology: Applications of High-Resolution EPR to Metalloenzymes*; Hanson, G., Berliner, L., Eds.; Biological Magnetic Resonance, Vol. 29; Springer: Berlin, 2010; pp 91–121.
- Pick, F. M.; McGartoll, M. A.; Bray, R. C. *Eur. J. Biochem.* **1971**, *18*, 65–72.
- Howes, B. D.; Bennett, B.; Bray, R. C.; Richards, R. L.; Lowe, D. J. *J. Am. Chem. Soc.* **1994**, *116*, 11624–11625.
- Howes, B. D.; Bray, R. C.; Richards, R. L.; Turner, N. A.; Bennett, B.; Lowe, D. J. *Biochemistry* **1996**, *35*, 1432–1443.
- Manikandan, P.; Choi, E.-Y.; Hille, R.; Hoffman, B. M. *J. Am. Chem. Soc.* **2001**, *123*, 2658–2663.
- Santos-Silva, T.; Ferroni, F.; Thapper, A.; Marangon, J.; Gonzalez, P. J.; Rizzi, A. C.; Moura, I.; Moura, J. J. G.; Romao, M. J.; Brondino, C. D. *J. Am. Chem. Soc.* **2009**, *131*, 7990–7998.
- Metz, S.; Wang, D.; Thiel, W. *J. Am. Chem. Soc.* **2009**, *131*, 4628–4640.
- Zhang, X.-H.; Wu, Y.-D. *Inorg. Chem.* **2005**, *44*, 1466–1471.
- Amano, T.; Ochi, N.; Sato, H.; Sakaki, S. *J. Am. Chem. Soc.* **2007**, *129*, 8131–8138.
- Howes, B. D.; Pinhal, N. M.; Turner, N. A.; Bray, R. C.; Anger, G.; Ehrenberg, A.; Raynor, J. B.; Lowe, D. J. *Biochemistry* **1990**, *29*, 6120–6127.
- Morpeth, F. F.; Bray, R. C. *Biochemistry* **1984**, *23*, 1332–1338.
- Turner, N. A.; Bray, R. C.; Diakun, G. P. *Biochem. J.* **1989**, *260*, 563–571.
- Pauff, J. M.; Zhang, J.; Bell, C. E.; Hille, R. *J. Biol. Chem.* **2008**, *283*, 4818–4824.
- Pauff, J. M.; Cao, H.; Hille, R. *J. Biol. Chem.* **2009**, *284*, 8760–8767.

- (16) Xanthine oxidase was prepared from unpasteurized milk as described in ref 17. ^2H and ^{13}C -labeled samples of H_2CO were obtained from Cambridge Isotopes and D_2O from Isotec, Inc. The 35 GHz pulsed EPR and ENDOR spectra were obtained as described in ref 18.
- (17) Massey, V.; Brumby, P. E.; Komai, H.; Palmer, G. *J. Biol. Chem.* **1969**, *244*, 1682–1691.
- (18) Lees, N. S.; Hänzelmann, P.; Hernandez, H. L.; Subramanian, S.; Schindelin, H.; Johnson, M. K.; Hoffman, B. M. *J. Am. Chem. Soc.* **2009**, *131*, 9184–9185.
- (19) Weber, S.; Kay, C. W. M.; Bacher, A.; Richter, G.; Bittl, R. *ChemPhysChem* **2005**, *6*, 292–299.
- (20) Kinney, R. A.; Hetterscheid, D. G. H.; Hanna, B. S.; Schrock, R. R.; Hoffman, B. M. *Inorg. Chem.* **2010**, *49*, 704–713.
- (21) Schweiger, A.; Jeschke, G. *Principles of Pulse Electron Paramagnetic Resonance*; Oxford University Press: Oxford, U.K., 2001.
- (22) Doan, P. E.; Lees, N. S.; Shanmugam, M.; Hoffman, B. M. *Appl. Magn. Reson.* **2010**, *37*, 763–779.
- (23) Stiefel, E. I.; Newton, W. E.; Pariyadath, N. *J. Less-Common Met.* **1977**, *54*, 513–525.
- (24) Miller, G. A.; McClung, R. E. D. *Inorg. Chem.* **1973**, *12*, 2552–2561.
- (25) Gelmini, L.; Stephan, D. W. *Organometallics* **1987**, *6*, 1515–1522.
- (26) Wang, W.; Wang, K.; Liu, Y.-L.; No, J.-H.; Li, J.; Nilges, M. J.; Oldfield, E. *Proc. Natl. Acad. Sci. U.S.A.* **2010**, *107*, 4522–4527.

JA106432H